Energy Conversion and Management 79 (2014) 721–730

Contents lists available at ScienceDirect

Energy Conversion and Management

journal homepage: www.elsevier.com/locate/enconman

Fifth harmonic and sag impact on PMSG wind turbines with a balancing new strategy for capacitor voltages

M. Seixas [a,b,c], R. Melício [a,b,*], V.M.F. Mendes [a,c,*]

[a] Department of Physics, Universidade de Évora, R. Romão Ramalho 59, 7002-554 Évora, Portugal
[b] IDMEC/LAETA, Instituto Superior Técnico, Universidade de Lisboa, Lisbon, Portugal
[c] Department of Electrical Engineering and Automation, Instituto Superior de Engenharia de Lisboa, R. Conselheiro Emídio Navarro, 1950-062 Lisbon, Portugal

ARTICLE INFO

Article history:
Received 12 October 2013
Accepted 31 December 2013
Available online 1 February 2014

Keywords:
Wind turbines
Permanent magnet generator
Unbalance voltage
Fractional-order controller
Electric grid
Power quality
Harmonic behavior

ABSTRACT

This paper deals with the computing simulation of the impact on permanent magnet synchronous generator wind turbines due to fifth harmonic content and grid voltage decrease. Power converter topologies considered in the simulations are the two-level and the three-level ones. The three-level converters are limited by unbalance voltages in the DC-link capacitors. In order to lessen this limitation, a new control strategy for the selection of the output voltage vectors is proposed. Controller strategies considered in the simulation are respectively based on proportional integral and fractional-order controllers. Finally, a comparison between the results of the simulations with the two controller strategies is presented in order to show the main advantage of the proposed strategy.

1. Introduction

Wind energy conversion (WEC) experienced a significant expansion worldwide [1–3]. Particularly, Europe made significant investments in WECs and most probably in the future will go ahead on developments. Even small European states experienced an expansion on WECs implementation, for instance, Portugal had a significant increase in installed capacity [4,5], which was the second highest share with 18% of wind power in 2010 [6]. A noteworthy day in 2010 was 31 of October with 61% of wind energy in the mixed conversion. High level of wind energy in the mixed conversion threatens the stability and power quality [7–9] in the electric grid. A simulation study is an important contribution required to take into account the behavior of WECs in order to evaluate not only grid stability, but also power quality injected into the grid [10]; anticipating in due course undesired behavior is an important security measure not to be disregarded. This paper in the following of other contributions [11–13] is a new contribution on power quality impact due to a grid voltage decrease and a fifth harmonic content.

A comparison of fixed speed wind turbine stabilization methods and guidelines for selection of a suitable technique for the stabilization of wind energy systems are reported in [14]. Nevertheless, the market share of the fixed-speed wind turbine has decreased in favor of the variable speed concept [15,16] due to the technical advantage in the variable speed for wind energy exploitation. Variable-speed wind turbines can be implemented in what regards power electronic with a partial-scale power converter, using a doubly fed induction generator [17–19], or with a full-scale power converter, using a synchronous generator. Higher costs are to be expected in the implementation with a full-scale power converter, but due to the advantage of performing a smooth grid connection over the entire speed range this implementation is a promising one. Variable-speed wind turbines can be implemented in what regards the direct-drive generators by an excited synchronous generator or by a permanent magnet synchronous generator (PMSG) [20]. Although large permanent magnets are costly, the PMSG has become a very interesting option in what regards the implementation of a variable speed wind generator [21], because of compact size, higher power density, reduced losses, high reliability and robustness [22], requiring no excitation circuit, so no additional DC supply. Moreover, a PMSG is almost maintenance free, because of the no need for slip rings usually requiring significant downtime maintenance. Also, due to the low rotational speed of synchronous generators the gearbox is not required. This is important not only due to less space need, but also for reducing the downtime failure [23,24] and because the gearbox

* Corresponding authors. Address: Department of Physics, Universidade de Évora, R. Romão Ramalho 59, 7002-554 Évora, Portugal. Tel.: +351 266 745372; fax: +351 266 745394 (R. Melício). Address: Department of Physics, Universidade de Évora, R. Romão Ramalho 59, 7002-554 Évora, Portugal (V.M.F. Mendes).
E-mail addresses: ruimelicio@uevora.pt (R. Melício), vfmendes@deea.isel.pt (V.M.F. Mendes).

0196-8904/$ - see front matter © 2014 Elsevier Ltd. All rights reserved.
http://dx.doi.org/10.1016/j.enconman.2013.12.067

Nomenclature

A_n	magnitude of the n eigenswing	ω_g	generator rotor speed
ω_n	eigenfrequency of the n eigenswing	J_g	generator moment of inertia
g_{nm}	distribution of the harmonic m in the n eigenswing	T_{dg}	generator bearing resistant torque
a_{nm}	normalized magnitude of g_{nm}	T_{ag}	airflow resistant torque in the generator
h_n	modulation of the n eigenswing	T_g	electric torque
φ_{nm}	phase of the harmonic m in the n eigenswing	i_f	equivalent rotor current
P_t	mechanical power of the wind turbine	M	mutual inductance
P_{tt}	mechanical power captured by the wind turbine without dynamic influences	p	number of pairs of poles
		i_d, i_q	stator dq currents
θ_i	pitch angle on blade $i \in \{1, 2, 3\}$	L_d, L_q	stator inductances
ω_t	wind turbine rotor angular speed.	R_d, R_q	stator resistances
J_t	wind turbine moment of inertia	v_d, v_q	stator voltages
T_t	mechanical torque	R_k	resistance of the electric grid
T_{dt}	wind turbine bearing resistant torque	L_k	inductance of the electric grid
T_{at}	airflow resistant torque in the hub and blades	v_{fk}	voltage at the filter
T_{ts}	stiffness torsional torque	v_k	voltage at the electric grid

usually requires significant maintenance. Power electronic efficiently compatibilize different electric power, plays an important role in WECs [25]. The three-level converters have emerge as a promising power converter interface [26] for WECs [27], allowing conversion in the megawatt range which is the current range for eolic turbines. However, three-level converters are limited by the following drawbacks: voltage unbalances, high component count, and increased control complexity [28]. A critical issue in multi-level converters, namely three-level converters, is related with the DC-link capacitors unbalance in the voltage, which may produce control malfunctions. A contribution in order to mitigate this critical issue is proposed for the three-level converters in this paper and considered in the simulation studies carried out in order to assess the effect on the electric current injected due to the presence of a grid voltage decrease and a fifth harmonic content. Although not imposed for WECs, the IEEE-519 imposes a total harmonic distortion (THD) not exceeding 5%, this THD is followed as a guideline for evaluation purpose of the performance achieved with the power electronic converters.

The rest of the paper is organized as follows. Section 2 presents the mechanical modeling, taking in consideration the dynamic associated with the action excited by wind on all physical structure and assuming a two-mass modeling for the rotor of the wind turbine and generator. Section 3 presents the electric modeling, considering PMSG with two converter configurations, respectively, two-level and three-level converter, and the modeling for the new balancing strategy in capacitors voltage. Section 4 presents notions about fractional calculus. Section 5 presents the controller modeling, using a classic PI and a fractional-order PI^{μ} controllers, and a new control strategy for the unbalancing in capacitors voltage. Section 6 presents two case studies using Matlab/Simulink language and respectively considering: grid ideal sinusoidal voltage or grid non-ideal voltage with decrease and fifth harmonic content. Finally, concluding notes are provided in Section 7.

2. Mechanical modeling

The wind speed is modeled by a finite sum of harmonic terms with frequencies range in 0.1–10 Hz and the mechanical power of the wind turbine is modeled taking in consideration three influences of the dynamic associated with the action excited by wind on all physical structure [29]. The mechanical power is given by:

$$P_t = P_{tt}\left[1 + \sum_{n=1}^{3} I_n(t)\right] \tag{1}$$

where

$$P_{tt} = \frac{1}{2}\rho\pi\, R^2\, u^3 c_p \tag{2}$$

The mechanical power in (1) is computed by a multiplicative term (2) given by the well-known formula for the mechanical power captured by the wind turbine without dynamic influences [11]. The influences considered are three, respectively: I_1 the asymmetry in the turbine, I_2 the vortex tower interaction and I_3 the eigenswings in the blades. Both influences are modeled by a sum given by:

$$I_n(t) = A_n\left(\sum_{m=1}^{2} a_{nm} g_{nm}(t)\right) h_n(t) \tag{3}$$

where

$$g_{nm}(t) = \sin\left(\int_0^t m\omega_n(t')dt' + \varphi_{nm}\right) \tag{4}$$

The dynamic associated with the asymmetry in the turbine is assessed considering the following data: $A_1 = 0.01$, $a_{11} = 4/5$, $a_{12} = 1/5$, $\omega_1(t) = \omega_t(t)$, $\varphi_{11} = 0$, $\varphi_{12} = \pi/2$. This influence is shown in Fig. 1

The dynamic associated with the vortex tower interaction is assessed considering the following data: $A_2 = 0.08$, $a_{21} = 1/2$, $a_{22} = 1/2$, $\omega_2(t) = 3\omega_t(t)$ $\varphi_{21} = 0$, $\varphi_{22} = \pi/2$. This influence is shown in Fig. 2.

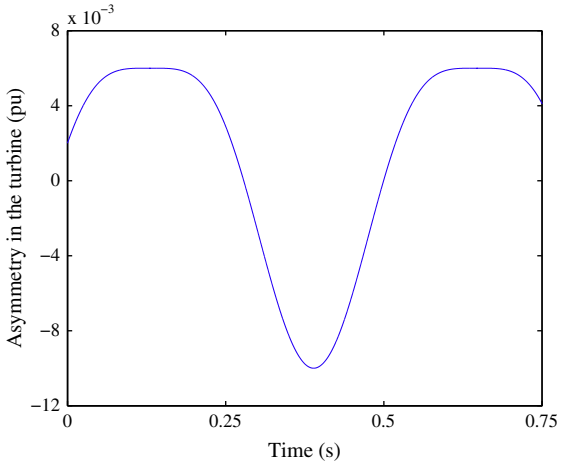

Fig. 1. Asymmetry in the turbine.

The dynamic associated with the eigenswings in the blades is assessed considering the following data: $A_3 = 0.15$, $a_{31} = 1$, $\omega_2(t) = 1/2[g_{11}(t) + g_{21}(t)]$, $\varphi_{31} = 0$. This influence is shown in Fig. 3.

The behavior of the mechanical drive train of a WEC can be considered by modeling the rotor as a set of discrete inertia masses connected together by springs and dampers. The two-mass model is the one followed in this paper. Hence, the equations for modeling the mechanical drive train are given by:

$$\frac{d\omega_t}{dt} = \frac{1}{J_t}(T_t - T_{dt} - T_{at} - T_{ts}) \tag{5}$$

$$\frac{d\omega_g}{dt} = \frac{1}{J_g}(T_{ts} - T_{dg} - T_{ag} - T_g) \tag{6}$$

This two-mass model has been proven as a good option, for instance, in [4] as a convenience to studying the behavior of the system in response to heavy disturbances.

3. Electric modeling

The equations for modeling a PMSG are shown in [30] and are given by:

$$\frac{di_d}{dt} = \frac{1}{L_d}(v_d + p\omega_g L_q i_q - R_d i_d) \tag{7}$$

$$\frac{di_q}{dt} = \frac{1}{L_q}\left[v_q - p\omega_g(L_d i_d + M i_f) - R_q i_q\right] \tag{8}$$

with the electric power P_g given by:

$$P_g = [\, v_d \quad v_q \quad v_f \,][\, i_d \quad i_q \quad i_f \,]^T \tag{9}$$

But in (9) due to the consideration of avowing demagnetization of the permanent magnet in the PMSG [31], a null stator current $i_d = 0$ has to be imposed.

The AC–DC–AC two-level converter and AC–DC–AC three-level converter are implemented respectively with twelve unidirectional commanded insulated gate bipolar transistors (IGBTs) and twenty-four unidirectional commanded IGBTs in order to implement the rectifier and the inverter functionality [13]. The configurations considered in this paper for the WECs with two-level and three-level converter are respectively shown in Figs. 4 and 5.

The modeling details regarding the two-level converter and the three-level converter with the unbalance formulation can be seen, for instance, in [4,5,13]. The advantages of the three-level over the two-level converters are identified [32] as a consequence of the increased number of voltage levels leading to the production of higher power quality waveforms [33], so the total harmonic distortion is expected to be lower. Also, the three-level converters are reported as a good trade off solution [34] between performance and cost in high-power systems. A survey of topologies, controls, and applications for three-level inverters is presented in [35].

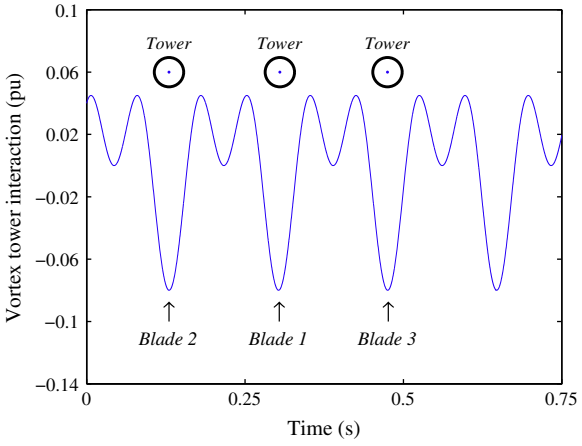

Fig. 2. Vortex tower interaction.

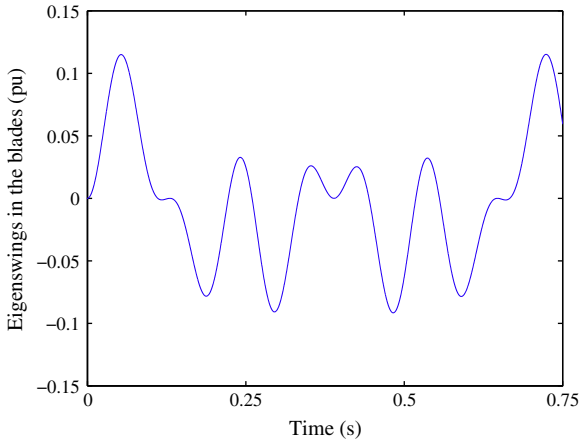

Fig. 3. Eigenswings in the blades.

The three-level converter is an AC–DC–AC converter, having twelve unidirectional commanded IGBTs identified by S_{ik}, used as a rectifier and with the same number of unidirectional commanded IGBTs used as an inverter. The rectifier is connected between the PMSG and a capacitor bank. The inverter is connected between this capacitor bank and a second order filter, which in turn is connected to an electric grid. The groups of four IGBTs linked to the same phase constitute the leg k of the converter.

The converter has $p = 3$ levels. For the new balance control strategy, the switching voltage level variable n_k which range from 0 to $(p-1)$ is used to identify the state of the IGBT i in the leg k of the converter establishing the switching function of each IGBT. The index i with $i \in \{1,2,3,4\}$ identifies the IGBT. The index k with $k \in \{1,2,3\}$ identifies the leg for the rectifier and $k \in \{4,5,6\}$ identifies the inverter one. The three valid conditions [36] for the switching voltage level variable of each leg k, at each level, are given by:

$$n_k = \begin{cases} 2, & (S_{1k} \text{ and } S_{2k}) = 1 \text{ and } (S_{3k} \text{ and } S_{4k}) = 0 \\ 1, & (S_{2k} \text{ and } S_{3k}) = 1 \text{ and } (S_{1k} \text{ and } S_{4k}) = 0 \\ 0, & (S_{3k} \text{ and } S_{4k}) = 1 \text{ and } (S_{1k} \text{ and } S_{2k}) = 0 \end{cases} \quad k \in \{1,\ldots,6\} \tag{10}$$

The switching voltage level variable n_k is also used to identify the vector (level-1) in the calculation of the converter output voltage v_{sk}.

The rectifier output line voltage v_{sij} is a function of v_{sk} and v_{mk} given by:

$$v_{sij} = v_{si} - v_{sj} = v_{mi} - v_{mj} \quad i,j \in \{1,2,3\} \quad \text{for } i \neq j \tag{11}$$

The difference between the line voltages is given by:

$$v_{mkj} - v_{mlk} = 2v_{mk} - \sum_{\substack{j=1 \\ j\neq k \\ k\neq l}}^{3} v_{mk} \quad k \in \{1,2,3\} \tag{12}$$

The rectifier output voltage v_{sk} in function of v_{dc} is given by:

$$v_{sk} = \frac{1}{6}\left(2n_k - \sum_{\substack{j=1 \\ j\neq k}}^{3} n_j\right) v_{dc} \quad k \in \{1,2,3\};\ n \in \{2,1,0\} \tag{13}$$

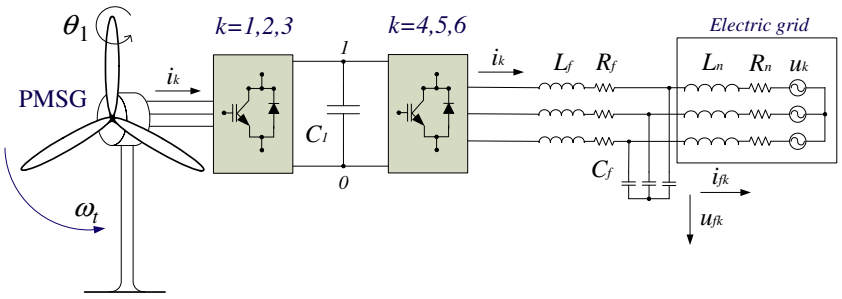

Fig. 4. WEC with two-level converter.

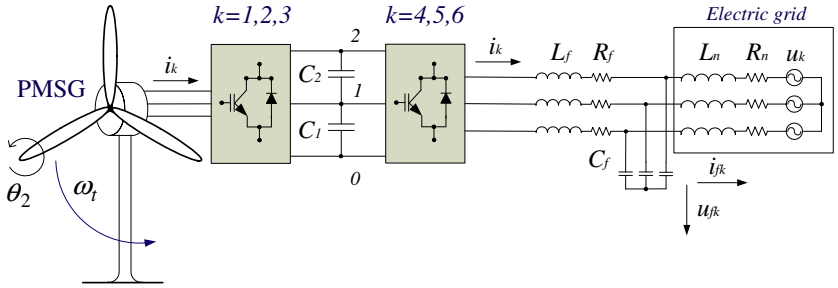

Fig. 5. WEC with three-level converter.

The methodology applied to the study of the inverter is similar to the rectifier. Consequently, the inverter output voltage is given by:

$$v_{sk} = \frac{1}{6}\left(2n_k - \sum_{\substack{j=1 \\ j\neq k}}^{3} n_j\right) v_{dc} \quad k \in \{4,5,6\};\ n \in \{2,1,0\} \tag{14}$$

For the old strategy [4] the switching variable γ_k is used to identify the state of the IGBT i in the leg k of the converter establishing the switching function of each IGBT. The three valid conditions [36] for the switching variable of each leg k are given by:

$$\gamma_k = \begin{cases} 1, & (S_{1k} \text{ and } S_{2k}) = 1 \text{ and } (S_{3k} \text{ and } S_{4k}) = 0 \\ 0, & (S_{2k} \text{ and } S_{3k}) = 1 \text{ and } (S_{1k} \text{ and } S_{4k}) = 0 \\ -1, & (S_{3k} \text{ and } S_{4k}) = 1 \text{ and } (S_{1k} \text{ and } S_{2k}) = 0 \end{cases} k \in \{1,\ldots,6\} \tag{15}$$

Auxiliary variables Φ_{1k} and Φ_{2k} are associated with IGBTs respectively with the upper and lower legs. Each auxiliary variable depends on the conduction and blockade states of the IGBTs and are defined in order to determine the electric current in the capacitors. These auxiliary variables Φ_{1k} and Φ_{2k} are function of the switching variable γ_k given by:

$$\Phi_{1k} = \gamma_k\left(\frac{\gamma_k + 1}{2}\right) \text{ and } \Phi_{2k} = \gamma_k\left(\frac{\gamma_k - 1}{2}\right) \text{ with } k \in \{1,\ldots,6\} \tag{16}$$

The capacitor voltage v_{dc} is the sum of the voltages v_{C1} and v_{C2} in the capacity banks C_1 and C_2, modeled by the state equation [36], given by:

$$\frac{dv_{dc}}{dt} = \frac{1}{C_1}\left(\sum_{k=1}^{3}\varphi_{1k}i_k - \sum_{k=4}^{6}\varphi_{1k}i_k\right) + \frac{1}{C_2}\left(\sum_{k=1}^{3}\varphi_{2k}i_k - \sum_{k=4}^{6}\varphi_{2k}i_k\right) \tag{17}$$

For the new balance control strategy, the current on each capacitor is given by:

$$i_{cj} = \sum_{k=1}^{3}\delta_{nk}i_k - \sum_{k=4}^{6}\delta_{nk}i_k \quad j \in \{1,\ldots,p-1\} \tag{18}$$

where the auxiliary variable δ_{nk} is given by:

$$\delta_{nk} = \begin{cases} 0 & j > n_k \\ 1 & j \le n_k \end{cases} \quad n \in \{2,1,0\};\quad j \in \{1,\ldots,p-1\} \tag{19}$$

The state equation of the voltage v_{dc} is given by:

$$\frac{dv_{dc}}{dt} = \sum_{j=1}^{p-1}\frac{1}{C_j}i_{cj} \quad j \in \{1,\ldots,p-1\} \tag{20}$$

The three-level converter with the new formulation is modeled by (10)–(14)and by (18)–(20).

A more detailed configuration of the rectifier for the three-level converter is shown in Fig. 6.

The electric grid is modeled by an equivalent three-phase active symmetrical circuit with a series of a resistance and an inductance. Hence, for electric current injected, see Figs. 4 and 5 into the electric grid the state equation are given by:

$$\frac{di_{fk}}{dt} = \frac{1}{L_n}(v_{fk} - R_n i_{fk} - v_k) \quad k = \{4,5,6\} \tag{21}$$

4. Fractional calculus

Fractional-order controller strategy is supported by the theory of Fractional calculus. Fractional calculus generalizes ordinary differentiation and integration calculus and it can be seen as the extension of it to include an arbitrary, non-integer order, including a complex order. Applications of fractional calculus theory in controller field have been proposed for WEC [5] in order to achieve a less harmonic content. The use of fractional-order PI^{μ} controllers can improve properties and controlling abilities over classical PI controllers [37].

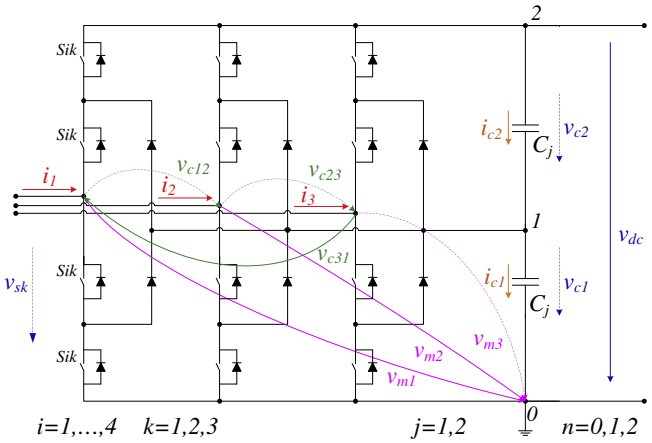

Fig. 6. Detailed configuration of the rectifier for the three-level converter.

The fractional-order operator denoted by ${}_aD_t^\mu$ [38] is given by:

$$ {}_aD_t^\mu = \begin{cases} \frac{d^\mu}{dt^\mu}, & \Re(\mu) > 0 \\ 1, & \Re(\mu) = 0 \\ \int_a^t (d\tau)^{-\mu}, & \Re(\mu) < 0 \end{cases} \tag{22} $$

where $\Re(\mu)$ is the real part of the μ, if $\Re(\mu) > 0$ then μ is the order of the derivative, if $\Re(\mu) < 0$ then $-\mu$ is the order of the integration.

Several approaches are possible for defining a fractional-order derivative and a fractional-order integral. The Riemann–Liouville definition is the most frequently encountered one. The Riemann–Liouville definition for the fractional-order derivative is given by:

$$ {}_aD_t^\mu f(t) = \frac{1}{\Gamma(n-\mu)} \frac{d^n}{dt^n} \left[\int_a^t \frac{f(\tau)}{(t-\tau)^{\mu-n+1}} d\tau \right] \tag{23} $$

where:

$$ \Gamma(x) \equiv \int_0^\infty y^{x-1} e^{-y} dy \tag{24} $$

while the definition of fractional-order integral is given by:

$$ {}_aD_t^{-\mu} f(t) = \frac{1}{\Gamma(\mu)} \int_a^t (t-\tau)^{\mu-1} f(\tau) d\tau \tag{25} $$

$\Gamma(x)$ is the Euler's Gamma function, a and t are the limits of the integration, and μ identifies the fractional order.

In this paper, μ is assumed as a real number that satisfies the restrictions $0 < \mu < 1$. Also, $a = 0$ and the following notational convention ${}_0D_t^{-\mu} \equiv D_t^{-\mu}$ are assumed.

Other used approach is Grünwald–Letnikov definition: for the fractional-order derivative given by:

$$ {}_aD_t^\mu f(t) = \lim_{\substack{h \to 0 \\ nh \approx t-a}} h^{-\mu} \sum_{r=0}^{n} (-1)^\mu f(t - rh) \tag{26} $$

for the fractional-order integral given by:

$$ {}_aD_t^{-\mu} f(t) = \lim_{h \to 0} h^\mu \sum_{r=0}^{\frac{t-a}{h}} \frac{\Gamma(\mu + r)}{r! \Gamma(\mu)} f(t - rh) \tag{27} $$

The fractional-order controller design is characterized in comparison with the classic one by having the additional advantage of augmenting the freedom for achieving an enhanced behavior [39], due to the advantage of having more criterion than the classical one, implied by the ability of weighting the past effects at each action of the controller. A fractional-order controller has a dynamical behavior described by a fractional differential integral equation with a derivative or an integral having at least a non-integer order.

5. Controller modeling

A classic controller *PI* and a fractional-order PI^μ controller implement respectively the two controller strategy considered in the simulation for the variable-speed operation of the wind turbine with PMSG and a full-power converter. The fractional-order PI^μ controller differential equation is given by:

$$ f(t) = K_p e(t) + K_i D_t^{-\mu} e(t) \tag{28} $$

The fractional-order PI^μ has the advantage of being more flexible than the classical *PI* controller. This advantage is due to the existence of one more adjustable parameter, accounting for the intensity of integration. The transfer function of the fractional-order controller, using the Laplace transform on (28), is given by:

$$ G(s) = K_p + K_i s^{-\mu} \tag{29} $$

Taking the order of integration μ equal to one in (29), a classical *PI* controller is obtained. The option [40] is followed for assessing the values of the parameters and circumvents the modeling of a mathematical programming problem, which is a different modeling. This type of option is the one normal in electric power systems to avoid a cumbersome modeling [24] for a fine tuning of parameters. The values of the parameters are given by a tradeoff compromised involving robustness and dynamic performance using tuning rules and favoring the range [0.4, 0.6] for the order of integration μ.

The design of PI^μ controller follows the tuning rules in [40]. Power converters are modeled as a pure delay [41] and the left-over dynamics are modeled with a second order equivalent transfer function, following the identification of a step response. The control strategy of the WEC with a three-level converter using PI^μ controllers has the block diagram shown in Fig. 7.

The voltage difference between v_{dc} and the reference v_{dc}^* is the input to the PI^μ controller in order to find the reference stator currents. While, the electric current difference between the stator current $i_{\alpha\beta}$ and the reference stator current $i_{\alpha\beta}^*$, is an error to be subjected to the input voltage vectors selection block given as an output of the commands for the three-level converter.

The convenient vector selection to ensure stability for the two-level and the three-level converter, with the old unbalance strategy, after being processed by the hysteresis comparator in the block of sliding mode control (SM) and space vector modulation (SVM) are given in [4,5,13].

The SM control is a lower level of control as is normally implemented with the PI controller, for controlling the converters is used Pulse width modulation by SVM associated with SM.

Physical constraints due to the power semiconductors have to be considered during design phase and simulation studies. Particularly, the constraint of power semiconductors due to the fact of having a non-infinite switching frequency, implying that an error on the electric current between the reference value and the control value have to be tolerated. For instances, finite value of switching frequency of 2 kHz, 5 kHz or 10 kHz are normally reported.

Based on the Concordia ($\alpha - \beta$) transformation, in order to guarantee that the system slides along the sliding surface $S(e_{\alpha\beta}, t)$, where $e_{\alpha\beta}$ is the error on the electric currents in the $\alpha\beta$-plane [42], is necessary to ensure that the state trajectory near the surface verifies the stability conditions given by:

$$ S(e_{\alpha\beta}, t) \frac{dS(e_{\alpha\beta}, t)}{dt} < 0 \tag{30} $$

The sliding surface in current practice is chosen in way to allow a small error $\varepsilon > 0$ for $S(e_{\alpha\beta}, t)$. This is due to power semiconductors

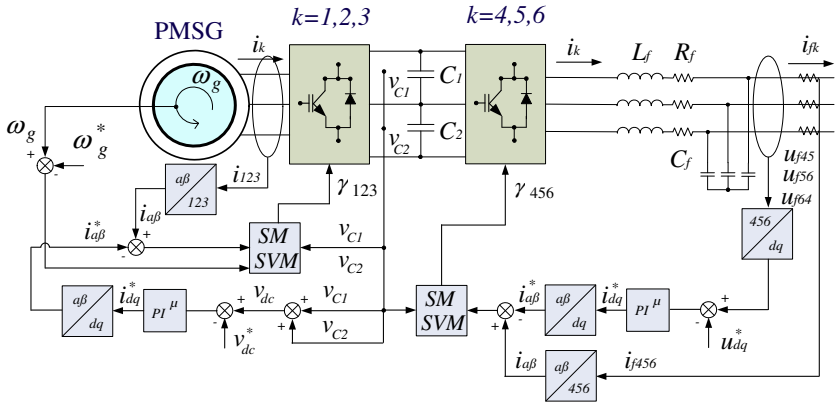

Fig. 7. Diagram of a WEC with three-level converter employing PI^{μ} controllers.

switching finite frequency. But, for the simulation studies, an implementation of the switching strategy considered may be implemented by hysteresis comparators performing accordingly to the condition given by:

$$-\varepsilon < S(e_{\alpha\beta}, t) < +\varepsilon \tag{31}$$

This implementation of the switching strategy is implemented in the SM, SVM block, see Fig. 7. The outputs of the hysteresis comparators are the integer variables $\sigma_{\alpha\beta} = (\sigma_\alpha, \sigma_\beta)$ [42]. For the two-level and the three-level converters, the output voltage vectors in the α β plane are shown in Fig. 8.

The integer voltage variables σ_α and σ_β are given by:

$$\sigma_\alpha, \sigma_\beta \in \{-2, -1, 0, 1, 2\} \tag{32}$$

In the old unbalance control strategy there are two tables of vectors selection, according to the capacitors voltages. If the upper capacitor is over loaded the input voltage vector is selected using the table that corresponds to the IGBTs states which discharges the upper capacitor and charges the lower capacitor. In the reverse situation, the other table is used [4,5]. In the new control strategy there are three output voltage vectors tables which take into account the voltage level of each capacitor bank, as shown in Fig. 8. For the three-level converter, the generic output voltage vector selection is shown in Table 1.

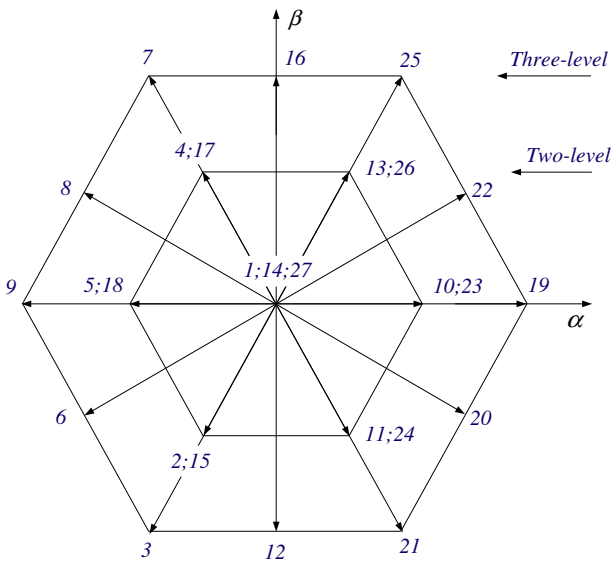

Fig. 8. Output voltage vectors for the three-level converter.

Table 1
Generic output voltage vectors selection for the three-level converter, with the redundant inner vectors.

$\sigma_\beta \setminus \sigma\alpha$	−2	−1	0	1	2
−2	3	3	12	21	21
−1	6	6; 2; 15	2; 15; 11; 24	11; 24; 20	20
0	9	5; 18	1; 14; 27	10; 23	19
1	8	8; 4; 17	4; 17; 13; 26	13; 26; 22	22
2	7	7	16	25	25

The integer voltage variables σ_α and σ_β allow choosing the most appropriate vector. On the inner output voltage vectors there are redundant ones corresponding to combinations of IGBT states, different from each other, which in turn correspond to a different voltage level selection. Thus the new control strategy mitigates the capacitors unbalancing voltages by selection of the most appropriate redundant vector, based on three tables, which define the vector to be used at each instant. Table 2 summarizes the vector selection for n = 0.

- Table 3 summarizes the vector selection for $n = 1$.
- Table 4 summarizes the vector selection for $n = 2$.

6. Case studies

The wind speed for the operational range of the WEC is in the region of 5–25 m/s and the switching frequency for IGBTs is 5 kHz. The data used for the mechanical eigenswings are given in [29]. A rated electric power of 900 kW is considered for the WEC, more data is in Table 5.

Following [40], the values $\mu = 0.5$, $K_p = 50$, $K_i = 2.6$ are used as input data in the simulations.

The three-level converter with the unbalancing formulation allows charging and discharging the capacitors voltage in order that their sum produces a dc voltage with the reference value. Ideally each of the capacitors is expected to contribute with half of the reference value. However, in practice, the voltage on each capacitor

Table 2
Output voltage vectors selection for the three-level converter, for $n = 0$.

$\sigma_\beta \setminus \sigma_\alpha$	−2	−1	0	1	2
−2	3	3	12	21	21
−1	6	2	2	20	20
0	9	5	1	10	19
1	8	4	4	22	22
2	7	7	16	25	25

Table 3
Output voltage vectors selection for the three-level converter, for $n = 1$.

$\sigma_\beta \setminus \sigma_\alpha$	−2	−1	0	1	2
−2	3	3	12	21	21
−1	6	15	11	11	20
0	9	5	14	23	19
1	8	17	13	26	22
2	7	7	16	25	25

Table 4
Output voltage vectors selection for the three-level converter, for $n = 2$.

$\sigma_\beta \setminus \sigma_\alpha$	−2	−1	0	1	2
−2	3	3	12	21	21
−1	6	6	24	24	20
0	9	9	27	23	19
1	8	8	26	26	22
2	7	7	16	25	25

Table 5
WEC data.

Turbine moment of inertia	2500×10^3 kg m^2
Turbine rotor diameter	49 m
Hub height	45 m
Tip speed	17.64–81.04 m/s
Rotor speed	6.9–31.6 rpm
Generator rated power	900 kW
Generator moment of inertia	100×10^3 kg m^2

deviates from the average value over time. The unbalancing voltage in the capacitor banks v_{C1} and v_{C2}, and the voltage v_{dc} are shown in Fig. 9.

The voltages in the capacitor banks with the new control strategy for the selection of the voltage vectors without unbalancing are shown in Fig. 10.

A comparison between Figs. 9 and 10 reveals the capability of the strategy in mitigating the unbalancing between the capacitors bank voltages.

The Discrete Fourier Transform is used to compute the total harmonic distortion THD given by:

$$\text{THD}\ (\%) = 100\frac{\sqrt{\sum_{H=2}^{50} X_H^2}}{X_F} \tag{33}$$

where X_H is the root mean square (RMS) value of the harmonic H, X_F is the RMS value of the fundamental component.

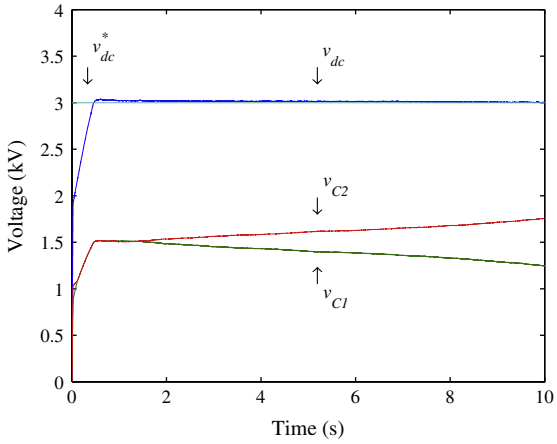

Fig. 9. Unbalancing voltage in capacitors.

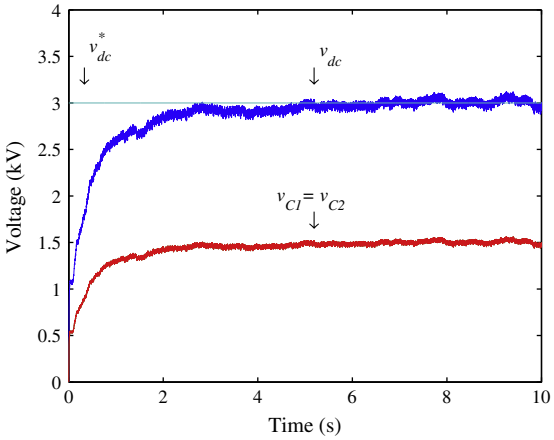

Fig. 10. Voltage without unbalancing in capacitors.

6.1. Case study 1 — grid ideal sinusoidal voltage

This case study considers the electric grid with highest energy quality and is a reference for Case study 2, which considers an electric grid voltage decrease and fifth harmonic in order to simulate a possible grid quality deficit. The electric grid has 850 V at 50 Hz. The mechanical power, the electric power, and the difference between these two powers, i.e., the accelerating power, are shown in Fig. 11.

The three influences shown in Figs. 1–3 are responsible by the behavior of the mechanical power (1) shown in Fig. 11, it is worth noting that due to the inertia of the rotor the electrical power is significantly free of those influences that are mainly presented in the accelerating power.

The results for the first harmonic and the fifth harmonic of the current injected into the electric grid for the WEC with the two-level converter are shown in Table 6.

A comparison between first harmonics and fifth harmonics in Table 6, shows that the PI^μ controllers are more favorable. The THD of the output current is shown in Fig. 12.

Again, by comparing the THD shown in Fig. 12, the PI^μ controllers are more favorable.

The first harmonic and the fifth harmonic of the current injected into the electric grid for the WEC with the three-level converter are shown in Table 7.

The PI^μ controller provides a greater first harmonic and less fifth harmonic than the PI controller as shown by comparing first

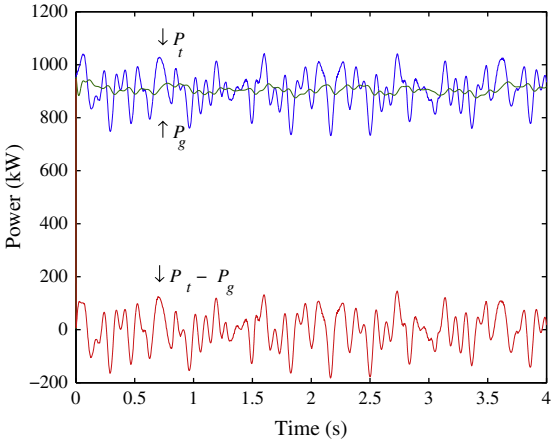

Fig. 11. Mechanical, electric and accelerating power.

Table 6
First harmonic and fifth harmonic of the current injected into the electric grid for the two-level converter.

Wind speed (m/s)	PI^{μ} controller		*PI* controller	
	First harmonic (%)	Fifth harmonic (%)	First harmonic (%)	Fifth harmonic (%)
5.0	93.8	0.43	93.1	0.49
7.5	94.2	0.26	93.3	0.34
10.0	94.3	0.18	93.4	0.21
12.5	94.3	0.18	93.5	0.21
15.0	94.3	0.17	93.5	0.21
17.5	94.4	0.17	93.5	0.21
20.0	94.4	0.17	93.5	0.2
22.5	94.4	0.17	93.5	0.2
25.0	94.4	0.17	93.5	0.2

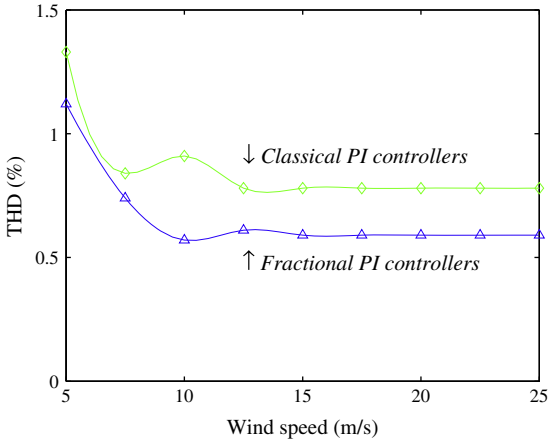

Fig. 12. THD of the output current, two-level converter.

Table 7
First harmonic and fifth harmonic of the current injected into the electric grid for the three-level converter.

Wind speed (m/s)	PI^{μ} controller		*PI* controller	
	First harmonic (%)	Fifth harmonic (%)	First harmonic (%)	Fifth harmonic (%)
5.0	94.07	0.33	94	0.38
7.5	94.19	0.21	94.06	0.27
10.0	94.38	0.17	94.14	0.19
12.5	94.78	0.16	94.28	0.19
15.0	94.94	0.14	94.45	0.17
17.5	95.18	0.14	94.63	0.17
20.0	95.18	0.14	94.82	0.17
22.5	95.2	0.14	94.82	0.17
25.0	95.24	0.14	94.82	0.17

harmonics and fifth harmonics in Table 7. The THD of the output current for the WEC with the three-level converter is shown in Fig. 13.

A comparison of Figs. 12 and 13 reveals that: the THD with the fractional-order controller strategy is never greater than the one with classical integer-order controller strategy; and the better performance of the three-level converter, which is able to achieve smaller THD values for wind speeds greater than 9 m/s. While the two-level converter is able to achieve lower THD values for wind speeds near the cut-in, less than 9 m/s, which are not the normal expected working wind speed.

6.2. Case study 2 — grid voltage decrease and fifth harmonic

This case study considers an electric grid voltage decrease and fifth harmonic in order to simulate a possible grid quality deficit.

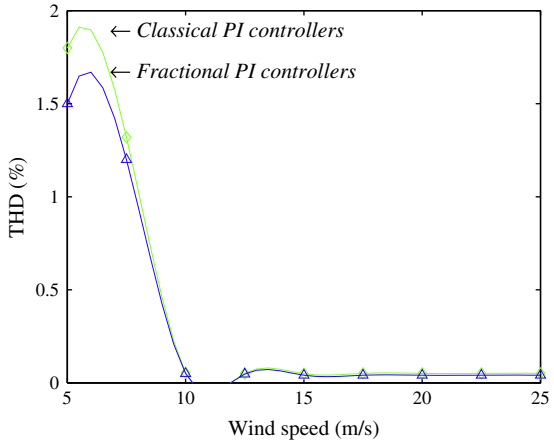

Fig. 13. THD of the output current, three-level converter.

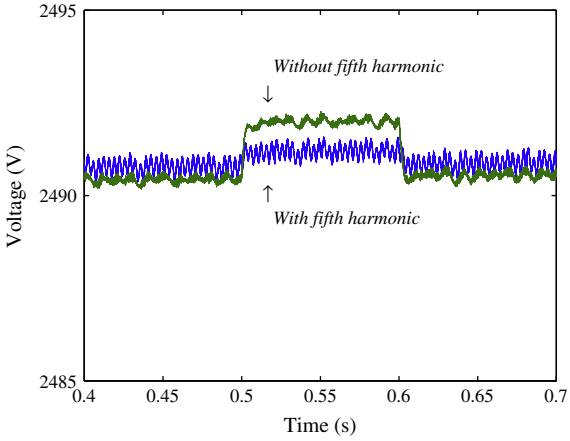

Fig. 14. Voltage v_{dc} during the grid voltage decrease, classical *PI* controller.

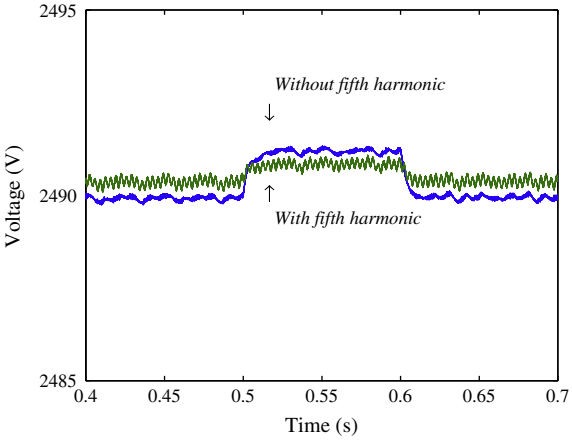

Fig. 15. Voltage v_{dc} during the grid voltage decrease, fractional controller.

The electric grid is characterized by 850 V at 50 Hz and 15% of fifth harmonic component. The time-domain simulation in order to see the behavior of the controller strategies on the voltage v_{dc} at the capacitor bank, green line without fifth harmonic, blue line with fifth harmonic, for *PI* controller and for PI^{μ} controller with a grid RMS voltage decreasing 25% during 100 ms are shown respectively in Figs. 14 and 15.

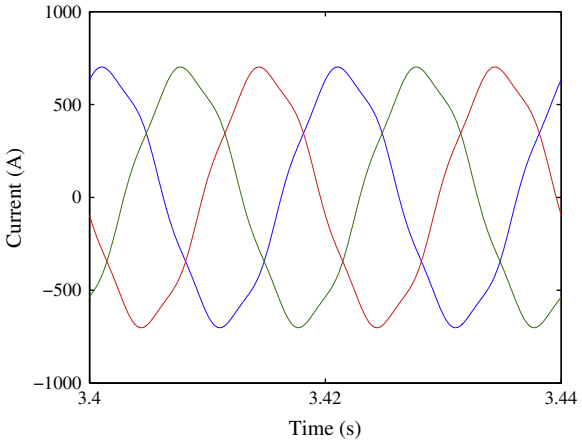

Fig. 16. Current injected in the grid for the three-level converter.

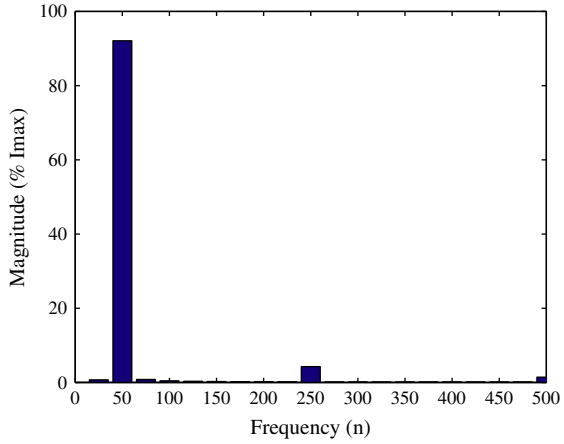

Fig. 17. DFT of the current injected into the grid for the three-level converter.

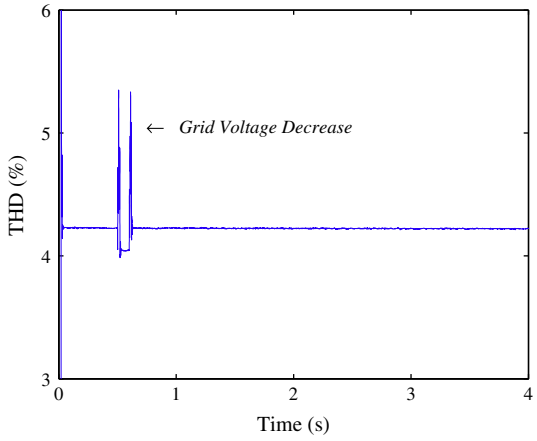

Fig. 18. THD of the output current, three-level converter.

The current injected in the grid for the three-level converter is shown in Fig. 16.

Fig. 16 shows that non-ideal sinusoidal voltage waveforms on the grid affect the waveform of the current at the output of the converters.

The harmonic behavior computed for the current injected in the grid with the three-level converter is shown in Fig. 17. The THD of the output current is shown in Fig. 18.

Table 8
THD of the current injected into the electric grid.

Wind power system with:	THD (%)	
	PI^{μ} controller	*PI* controller
Two-level converter	5.16	5.89
Three-level converter	4.21	4.75

Fig. 17 shows that for the non-ideal sinusoidal voltage waveform on the grid the dominant harmonics on the current inject into the electric grid are the 5th and the 10th order harmonics. The interharmonics of other orders namely subharmonics of odd order and harmonics of even order have a negligible magnitude.

The average THD of the current injected into the electric grid for the two-level and three-level converters are shown in Table 8.

With the three-level converter, the THD of the output current is lower than the 5% limit imposed by IEEE-519 standard [43].

7. Conclusions

The new formulation for the electrical modeling of the three-level converter combined with the new control strategy reveals the capability in mitigating the unbalancing between the capacitors bank voltages. The THD of the output current with the two-level converter and with the three-level converter have propensity to be decremented with the increment on the wind speed. The ideal sinusoidal voltage waveforms on the grid gives as expected smaller values for the THD, lower than 5% limit imposed by IEEE-519 standard, in comparison with non-ideal sinusoidal voltage waveforms having a fifth harmonic. Hence, non-ideal sinusoidal voltage waveforms on the grid affect the current injected into the grid by the WEC. The fractional-order controller strategy provides better results comparatively with the classic controller in what regards the level of the first harmonic and the THD. The fractional-order controller strategy provides better results when comparing with the classical integer-order controller strategy in what regards a time-domain simulations performance by means of sudden grid RMS voltage decrease. The WEC with three-level converter for grid voltage with 15 % of fifth harmonic, the THD is lower than 5% limit imposed by IEEE-519 standard. Finally, the values of THD should not only be imputed as a responsibility of the WEC, but also of the electric grid due to the presence of an endogenous voltage fifth harmonic component.

Acknowledgments

This work was partially supported by Fundação para a Ciência e a Tecnologia, through IDMEC under LAETA, Instituto Superior Técnico, Universidade de Lisboa, Portugal.

References

[1] Mostafeipour A. Economic evaluation of small wind turbine utilization in Kerman, Iran. Energy Conversion Manage 2013;73:214–25.
[2] Aissaoui AG, Tahour A, Essounbouli N, Nollet F, Abid M, Chergui MI. A fuzzy-PI control to extract an optimal power from wind turbine. Energy Conversion Manage 2013;65:688–96.
[3] Tsang KM, Chan WL. Three-level grid-connected photovoltaic inverter with maximum power point tracking. Energy Conversion Manage 2013;65:221–7.
[4] Melício R, Mendes VMF, Catalão JPS. Fractional-order control and simulation of wind energy systems with PMSG/full-power converter topology. Energy Conversion Manage 2010;51:1250–8.
[5] Melício R, Mendes VMF, Catalão JPS. Behaviour of PMSG wind turbines with fractional controllers to a voltage decrease in the grid. In: Proc. 6th IET international conference on power electronics, Machines and drives, Bristol, UK, 2012. p. 1–5.
[6] World Wind Energy Report 2010, 10th World Wind Energy Conf. Ren Energy Exhibition, Cairo, Egypt, 2011.

[7] Ge B, Wang W, Bi D, Rogers CB, Peng FZ, de Almeida AT. Energy storage system-based power control for grid-connected wind power farm. Elec Power Energy Syst 2013;44:115–22.
[8] Cucchiella F, Adamo I. Issue on supply chain of renewable energy. Energy Conversion Manage 2013;76:774–80.
[9] Mohammadi J, Afsharnia S, Vaez-Zadeh S. Efficient fault-ride-through control strategy of DFIG-based wind turbines during the grid faults. Energy Conversion Manage 2014;78:88–95.
[10] Muyeen SM, Hasanien HM, Al-Durra A. Transient stability enhancement of wind farms connected to a multi-machine power system by using an adaptive ANN-controlled SMES. Energy Conversion Manage 2014;78:412–20.
[11] Melício R, Mendes VMF, Catalão JPS. Harmonic assessment of variable-speed wind turbines considering a converter control malfunction. IET Renew Power Gener 2010;4:139–52.
[12] Melício R, Mendes VMF, Catalão JPS. Comparative study of power converter topologies and control strategies for the harmonic performance of variable-speed wind turbine generator systems. Energy 2011;36:520–9.
[13] Melício R, Mendes VMF, Catalão JPS. Wind turbines with permanent magnet synchronous generator and full-power converters: modeling, control and simulation. In: Al-Bahadly Ibrahim, editor. Wind turbines. Vienna, Austria: In-Tech; 2011. p. 465–94.
[14] Ali MH, Wu B. Comparison of stabilization methods for fixed-speed wind generator systems. IEEE Trans Power Deliv 2010;25:323–31.
[15] Li H, Chen Z. Overview of different wind generator systems and their comparisons. IET Renew Power Gener 2008;2:123–38.
[16] Hong C-M, Chen C-H, Tu C-S. Maximum power point tracking-based control algorithm for PMSG wind generation system without mechanical sensors. Energy Conversion Manage 2013;69:58–67.
[17] Wang Y, Xu L. Coordinated control of DFIG and FSIG-based wind farms under unbalanced grid conditions. IEEE Trans Power Deliv 2010;25:367–77.
[18] Fan LL, Kavasseri R, Miao ZL, Zhu CX. Modeling of DFIG-based wind farms for SSR analysis. IEEE Trans Power Deliv 2010;25:2073–82.
[19] Melicio R, Mendes VMF. Doubly fed induction generator systems for variable speed wind turbine. In: Proc. 9th Spanish–Portuguese congress on electrical engineering, Marbella, Spain, 2005. p. 161–164.
[20] El-Khattam W, Yazdani A, Sidhu TS, Seethapathy R. Investigation of the local passive anti-islanding scheme in a distribution system embedding a PMSG-based wind farm. IEEE Trans Power Deliv 2011;26:42–52.
[21] Muyeen SM, Takahashi R, Tamura J. Operation and control of HVDC-connected offshore wind farm. IEEE Trans Sust Energy 2010;1:30–7.
[22] Singh M, Khadkikar V, Chandra A. Grid synchronisation with harmonics and reactive power compensation capability of a permanent magnet synchronous generator-based variable speed wind energy conversion system. IET Power Electron 2011;4:122–30.
[23] Ribrant J, Bertling LM. Survey of failures in wind power systems with focus on Swedish wind power plants during 1997–2005. IEEE Trans Energy Convers 2007;22:167–73.
[24] Muyeen SM, Al-Durra A, Tamura J. Variable speed wind turbine generator system with current controlled voltage source inverter. Energy Conversion Manage 2011;52:2688–94.
[25] Chen Z, Guerrero JM, Blaabjerg F. A review of the state of the art of power electronics for wind turbines. IEEE Trans Power Electron 2009;24:1859–75.
[26] Gupta KK, Jain S. A multilevel voltage source inverter (VSI) to maximize the number of levels in output waveform. Elec Power Energy Syst 2013;44:25–36.
[27] Kouro S, Malinowski M, Gopakumar K, Pou J, Franquelo LG, Wu B, et al. Recent advances and industrial applications of multilevel converters. IEEE Trans Ind Electron 2010;57:2553–80.
[28] Portillo RC, Prats MM, León JI, Sanchez JA, Carrasco JM, Galván E, et al. Modeling strategy for back-to-back three-level converters applied to high-power wind turbines. IEEE Trans Ind Electron 2006;53:1483–91.
[29] Akhmatov V, Knudsen H, Nielsen AH. Advanced simulation of windmills in the electric power supply. Int J Electr Power Energy Syst 2000;22:421–34.
[30] Ong C-M. Dynamic simulation of electric machinery: using Matlab/Simulink. New Jersey: Prentice-Hall; 1998. p. 259–350.
[31] Senjyu T, Tamaki S, Urasaki N, Uezato K. Wind velocity and position sensorless operation for PMSG wind generator. In: Proc. 5th Int. Conf. on Power Electronics And Drive Systems, Singapore, 2003. p. 787–792.
[32] Nabae A, Takahashi I, Akagi H. A new neutral-point-clamped PWM inverter. IEEE Trans Ind Appl 1981;17:518–23.
[33] Babaei E, Hosseini SH, Gharehpetian GB, Haque MT, Sabahi M. Reduction of dc voltage sources and switches in asymmetrical multilevel converters using a novel topology. Electr Power Syst Res 2007;77:1073–85.
[34] Alepuz S, Busquets-Monge S, Bordonau J, Gago J, Gonzalez D, Balcells J. Interfacing renewable energy sources to the utility grid using a three-level inverter. IEEE Trans Ind Electron 2006;53:1504–11.
[35] Rodriguez J, Lai JS, Peng FZ. Multilevel inverters: a survey of topologies, controls, and applications. IEEE Trans Ind Electron 2002;49:724–38.
[36] Barros JD, Silva JF. Optimal predictive control of three-phase NPC multilevel converter for power quality applications. IEEE Trans Ind Electron 2008;55:3670–81.
[37] Arijit B, Swagatam D, Ajith A, Sambarta D. Design of fractional-order PI-lambda-D-mu-controllers with an improved differential evolution. Eng Appl Artif Intell 2009;22:343–50.
[38] Calderón AJ, Vinagre BM, Feliu V. Fractional order control strategies for power electronic buck converters. Signal Process 2006;86:2803–19.
[39] Biswas A, Das S, Abraham A, Dasgupta S. Design of fractional-order (PID mu)-D-lambda controllers with an improved differential evolution. Eng Appl Artif Intel 2009;22:343–50.
[40] Maione G, Lino P. New tuning rules for fractional PI-alfa controllers. Nonlinear Dynamics 2007;49:251–7.
[41] Chinchilla M, Arnaltes S, Burgos JC. Control of permanent–magnet generators applied to variable-speed wind energy systems connected to the grid. IEEE Trans Energy Convers 2006;21:130–5.
[42] Silva J, Pinto S. Control methods for switching power converters. In: Rashid MH, editor. Power electronics handbook. New York: Academic Press; 2007. p. 935–98.
[43] IEEE Guide for Harmonic Control and Reactive Compensation of Static Power Converters, IEEE Standard 519-1992, 1992.